Appendix A

Evidences for aseismic slip in the seismogenic depth range, in other geological contexts

Measurements of surface deformation have shown that stress on faults is either released seismically or as aseismic slip, called fault creep. This has been observed along a number of subduction zones including Japan, Sumatra, Peru, Chile and Alaska (*e.g. Freymueller et al.*, 2000; *Igarashi et al.*, 2003; *Chlieh et al.*, 2008; *Moreno et al.*, 2008; *Hashimoto et al.*, 2009; *Kaneko et al.*, 2010), but also on continental faults such as in California, Turkey, the Philippines, China and Taiwan (e.g. *Thomas et al.*, to be submitted; *Titus et al.*, 2006; *Galehouse and Lienkaemper*, 2003; *Richards-Dinger and Shearer*, 2000; *Jolivet et al.*, 2012; *Kaneko et al.*, 2013; *Duquesnoy et al.*, 1994). In this section we review continental faults for which aseismic creep occurs in the seismogenic zone.

A.1 San Andreas Fault system, California

Creep on the San Andreas fault (SAF) system, which is a major component of the active transform plate boundary between the North America and the Pacific Plates (*Chester et al.*, 1993), has been monitored at several locations.

Although anticipated by *Louderback* (1942), creep was not observed in California until the early 1960s (*Steinbrugge and Zacher*, 1960; *Tocher*, 1960), when very localized deformed anthropogenic features were observed at a winery near Hollister, California. This 175-km-long Parkfield creeping segment of the SAF, between San Juan Bautista and Cholame, separates the locked sections of the fault that ruptured during the Fort Tejon earthquake of 1857 and the San Francisco earthquake of 1906 (*Titus et al.*, 2006). Following the recognition of aseismic slip on that fault, periodic and continuous measurement of creep have been performed using alignment arrays (*Burford and Harsh*, 1980; *Lienkaemper and Prescott*, 1989; *Titus et al.*, 2005, 2006), trilateration networks (*Lisowski and Prescott*, 1981; *Prescott et al.*, 1981; *Lienkaemper and Prescott*, 1989), creepmeters (*Schulz et al.*,

1982; *Titus et al.*, 2006; *Lienkaemper and Prescott*, 1989), GPS (*Langbein and Bock*, 2004; *Titus et al.*, 2005, 2006; *Rolandone et al.*, 2008) and InSAR data (*Ryder and Burgmann*, 2008; *de Michele et al.*, 2011). A combination of geodetic measurements have demonstrated that faster slip rates are observed at greater distances from the fault. Creepmeters and alignment arrays document an average minimum creep rate of 21-26 mm/yr on the fault trace. Motion between continuous GPS sites return 28.2 ± 5.0 mm/yr for two sites 1 km apart and 33.6 ± 5.0 mm/yr for two sites that are 70 km apart (*Titus et al.*, 2006). This pattern implies that either part of the deformation occurs off the San Andreas Fault or that strain accumulates along the creeping segment due to partial coupling on the fault, or some combination thereof (*Titus et al.*, 2006). The good agreement between today's measurement from cGPS stations 1 km apart and geological slip rate estimates at Wallace Creek, California (34 ± 3 mm/yr) (*Sieh and Jahns*, 1984), implies little or no interseismic stress build-up to be released seismically on the creeping section. Moreover, all creeping rate measurements are slower than the 39 ± 2 mm/yr predicted motion between the Sierra Nevada-Great Valley Block and the Pacific Plate. Therefore, deformation must occur off the San Andreas Fault, either seismically or aseismically. Detailed mapping of the spatio-temporal evolution of aseismic creep on the Parkfield segment are found in recent published papers based on geodetic, seismological and/or remote sensing data (e.g. *Nadeau and McEvilly*, 1999; *Murray et al.*, 2001; *Titus et al.*, 2006; *Ryder and Burgmann*, 2008; *Barbot et al.*, 2009; *de Michele et al.*, 2011; *Tong et al.*, 2013).

In the San Francisco Bay Area (SFBA), motion between the Pacific Plate and Sierra Block is partitioned across 7 major subparallel right-lateral faults with < 20 km spacing (e.g. *Freymueller et al.*, 1999; *Evans et al.*, 2012). From West to East these include the San Gregorio, the San Andreas, the Hayward, the Rodgers Creek, the Calaveras, the Concord/Green Valley and the Greenville Faults. The San Andreas Fault is fully locked northwest from San Juan Bautista, *i.e*, at the southern end of the 1906 earthquake rupture (*Galehouse and Lienkaemper*, 2003). Likewise, the San Gregorio fault shows no creep. On the other end, several faults within the SFBA have long been known to exhibit interseismic creep, including the Hayward Fault (4.6 mm/yr) (*Prescott et al.*, 1981; *Lienkaemper et al.*, 1991; *Schmidt et al.*, 2005; *Kanu and Johnson*, 2011; *Evans et al.*, 2012), the Calaveras Fault (14 ± 2 in south, ~ 10 mm/yr in the central part and 3-4 mm/yr in north)(*Rogers and D.*, 1971; *Prescott et al.*, 1981), the Concord Fault (2.5-3.5 mm/yr) and its northward continuation, the Green Valley Fault (4.4 mm/yr) (*Galehouse and Lienkaemper*, 2003). More recently, PS-InSAR data from *Funning et al.* (2007) has demonstrated that aseismic creep also occurs on the Rodgers Creek Fault, at a rate up to 6 mm/yr. This particular fault is aligned with the Hayward Fault (South) and the Maacama Fault (North) which has been proved to slip aseismically as well (4.4 to 6.5 mm/yr) (*Galehouse and Lienkaemper*, 2003). Based on two decades of alinement array measurements of creep in the SFBA, *Galehouse and Lienkaemper* (2003) have demonstrated that if the central and southern segments of the Calaveras Fault are predominantly creeping, the Hayward Fault, the Northern

Calaveras Fault and the Maacama Fault are partly locked, generating sufficient elastic strain to produce major earthquakes. Indeed, the Hayward Fault generated a severely damaging earthquake (M 6.8) in 1868 with a reported surface rupture from Fremont in the South to San Leandro in the North (*Evans et al.*, 2012). Based on seismic and geodetic data, the partial coupling of the Hayward Fault has been discussed furthermore by *Schmidt et al.* (2005) and *Evans et al.* (2012).

Finally, trilateration network have revealed aseismic slip on the southern section of the San Andreas fault system (*Louie et al.*, 1985). The Banning, Coyote Creek, Imperial and Superstition Hills fault have been recognized to creep but at the time of survey some of the one-going slip could have been related to the postseismic relaxation following the 1979 Imperial Valley and 1968 Borrego Mountain earthquakes (*Louie et al.*, 1985). Recent permanent scattereers InSAR study by *Lyons and Sandwell* (2003) along the seismic gap on San Andreas fault near the Salton Sea (*Richards-Dinger and Shearer*, 2000) reveal a diffuse secular strain buildup, punctuated by localized interseismic creep of 4-6 mm/yr line of sight, 12-18 mm/yr horizontally (if assumed pure strike-slip motion). This section of the San Andreas fault has undergone four large slip events between 1000 and 1700 A.D. (*Sieh*, 1986) with a reccurence interval of about 230 years. The last major events has been inferred to have happened in 1700 (*Sieh*, 1986), therefore significant seismic event along this portion of the San Andreas Fault is consider to be overdue (*Lyons and Sandwell*, 2003).

A.2 Haiyuan Fault, Gansu, China

The Haiyuan Fault is part of a major left-lateral fault system at the northeastern edge of the Tibet-Qinghai plateau. Two M_w 8 earthquakes ruptured locked sections of this fault system in the last century (1920 and 1927), bracketing an unbroken section of the fault identified as the Tianzhu seismic gap (*Gaudemer et al.*, 1995). Interferometric synthetic aperture radar data have been used to infer interseismic velocity field along the Haiyuan Fault system, and they revealed the existence of a shallow, 35 km-long, slipping zone near the junction between the Tianzhu seismic gap and the fault section, which broke in the 1920, M_w 8 Haiyuan earthquake (*Cavalie et al.*, 2008; *Jolivet et al.*, 2012). Inferred average shallow slip-rate ($\sim$ 5 mm/yr) is comparable in magnitude with the estimated loading rate at depth, assumed to be constant along the fault (*Jolivet et al.*, 2012).

A.3 North Anatolian Fault, western Turkey

Evidence of creep along the North Anatolian Fault (NAF) at Ismetpasa (Turkey) was first mentioned by *Ambraseys* (1970), but until the last decade little was known about its lateral extent and rate. InSAR studies and elastic dislocation models have revealed discontinuities of up to $\sim$ 5 mm/yr across the Ismetpasa segment of the NAF, implying surface creep at a rate of $\sim$ 9 mm/yr (*Kaneko et al.*,

2013) or 8 ± 3 mm/yr based on *Cakir et al.* (2005). This is a large fraction of the inferred long-term slip rate of the NAF (22 ± 3 mm/year) (*McClusky et al.*, 2000). The lateral extent of significant surface creep is about 75 km, starting at the western termination of the Tosya 1943 (M = 7.6) earthquake rupture (*Barka*, 1996) and overlapping with the eastern part of the 1944 Bolu-Gerede (M = 7.3) earthquake rupture (*Barka*, 1996; *Cakir et al.*, 2005; *Kaneko et al.*, 2013). Instrumental measurements (*i.e.*, local triangulation networks and creepmeters) between 1982-1992 give a rate of 7.7 ± 1.1 mm/yr (*Deniz et al.*, 1993), which is in good agreement with the InSAR data (*Cakir et al.*, 2005). Ground-based LiDAR measurements ($6.0 - 10.1 \pm 4.0$ mm/yr) are also consistent with other datasets (*Karabacak et al.*, 2011). It is not known whether or not the fault was creeping before the 1944 earthquake. However, based on the study of *Cakir et al.* (2005), the rate of creep appears to have exponentially decreased with time since 1944, suggesting that creep may have started after the Bolu-Gerede event as postseismic relaxation, and hence aseismic slip on the NAF is transient.

More recently, SAR and GPS measurements reveal afterslip displacement triggered by the 1999 M7.4 earthquake that progressively slowed down to reach a steady rate ten years after the earthquake with a rate comparable to the pre-earthquake rate (*Cakir et al.*, 2012; *Reilinger et al.*, 2000; *Ergintav et al.*, 2009).

A.4 Philippine Fault system, Leyte island

Geodetic, trilateration and GPS measurements in the central part of the Philippine Fault system on Leyte island (Philippines) have revealed asesimic creep at a rate of at least 26 mm/yr (left-lateral) on two segments: the north Central Leyte Fault and the south Central Leyte Fault (*Duquesnoy et al.*, 1994; *Besana and Ando*, 2005). Creep in this particular case is believed to be linked to the mechanical strength of the crust, which is supposed to be weak in this area where the fault intersects the volcanic arc. High geothermal gradient and strong geothermal flows are also observed there (*Duquesnoy et al.*, 1994).

A.5 Asal Rift, Djibouti

Interferometry study in the Asal Rift (Djibouti) has revealed that creep behavior can also occur on normal faults (*Doubre and Peltzer*, 2007). Surface displacement maps show that the asysmmetric subsidence of the inner floor of the rift (with respect to the bordering shoulders) is accommodated by three main active faults. Slip on faults occurs either as steady creep or during sudden slip events conjointly with an increase in seismicity. *Doubre and Peltzer* (2007) suggest that slip on the faults is controlled by the small pressure changes in fluid-filled fractures connected to the faults.

A.6 Geological setting and aseismic behavior

These examples show that aseismic creep can occur in a variety of geological settings (e.g., *Graymer et al.*, 2005; *Holdsworth et al.*, 2011; *Bradbury et al.*, 2007; *Janssen et al.*, 2012, and chapter 3). While no systematics arise from this compilation, one might note that some of these examples involved subduction zone formations (e.g., *Holdsworth et al.*, 2011; *Huang et al.*, 2006a; *Teng*, 1980a). This observation comforts the view that subduction related clay-rich mélanges favor the occurrence of aseismic creep patches. By contrast, continental clastic formations seem to result in settings that are generally well locked in the 0-20km depth range (*Ader et al.*, 2012; *Hsu et al.*, 2009a). It also seems that the hythrothermalism in volcanic contexts favors aseismic creep, as the Philippine Fault through Leyte island and the Asal rift examples suggest (*Doubre and Peltzer*, 2007; *Duquesnoy et al.*, 1994; *Besana and Ando*, 2005). This would be consistent with the general observation that the ridge and transform faults in the oceanic lithosphere setting are dominantly aseismic (e.g., *Bird and Kagan*, 2004).

Appendix B

A brief review of rock deformation mechanisms

A number of mechanisms could potentially contribute to aseismic deformation. We briefly review these mechanisms, the conditions under which they operate (depending on temperature, strain rate, stress, confining pressure, grain size and chemical composition) and the criteria which might be used to detect them from observation of fault-zone rocks. They include cataclastic flows, pressure solution creep, dislocation creep, diffusion creep, and granular flow (*Snoke et al.*, 1998). Each mechanism displays a characteristic set of microstrutures, occurs at a specific set of pressure-temperature-fluid conditions (over which it is dominant) and displays a distinct form of flow law (*Snoke et al.*, 1998). Most of these mechanisms result in non-linear flow laws of the form:

$$\dot{\epsilon} = A\frac{\sigma^n}{d^m}\exp\left(\frac{Q}{RT}\right), \tag{B.1}$$

describing how the stress rate, $\dot{\epsilon}$, depends on the differential stress, σ, and grain size, d. The various mechanisms differ in the exponent n, dependency on grain size, represented by the exponent m, and activation energy Q. The diagram below qualitatively maps the domains of operation of these mechanisms as a function of strain rate and differential stress level (modified from *Davis et al.* (1996)). Similar diagrams that consider strain rates and grain size as mapping variables can be found in the literature.

B.1 Granular flows

Granular flows involve the rolling and sliding of rigid particles (relative to each other) of unlithified sediments layers or slurries (*Gifkins*, 1976; *Twiss and Moores*, 1992; *Stunitz and Gerald*, 1993). It occurs only at low effective confining pressures and involves friction; therefore it is an upper surface process, unless high pore fluid pressure lowers the effective confining pressure by reducing σ_n. Granular flow is an important soft-sediment deformation mechanism that must play a predominant role

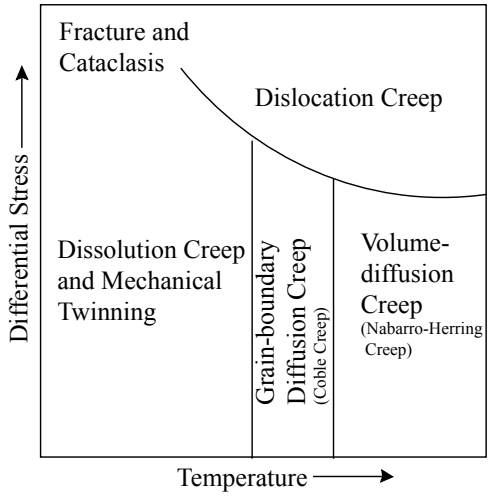

Figure B.1: Simplified deformation mechanism maps (Modified from *Davis et al.* (1996)). Plot of differential stress vs temperature, showing the field in which different mechanisms dominate relative to one another.

in deforming accretionary prisms in subduction zones (*Twiss and Moores*, 1992). Grains themselves show no evidence of granular flow (no characteristic microfabrics), only rocks are deformed. Hence, it is a mechanism difficult to detect based on the structural observation of fault-rocks.

B.2 Cataclastic flows

Cataclastic flow, in which crystal structure remains undistorted, involves continuous brittle fracturing and communition of grains with frictional sliding and rolling of the fragments with respect to one another (*Engleder*, 1974; *Rutter*, 1986; *Twiss and Moores*, 1992; *Hadizadeh et al.*, 2012). The process necessarily involves dilatancy and is therefore pressure sensitive (*Rutter*, 1986). This is a mechanism that operates under low to moderate temperatures, low confining pressure and relatively high strain rates, which leads to a progressive diminution of grain size (*Twiss and Moores*, 1992). Cataclastic flow occurs instead of granular flow when effective confining pressure is too high to promote granular flow, *i.e*, when the work required to fracture grains is less that the work required to slide or roll them past one another (*Twiss and Moores*, 1992). In term of microfabrics, cataclasis are characterized by the presence of pervasive cracks and sharp angular clasts/grains which can be very different in size, and commonly by the absence of any foliation (*Twiss and Moores*, 1992).

B.3 Stress corrosion

Stress corrosion is the growth of cracks associated with chemical reactions of the host material. It involves atomic bond rupture enhanced by stress and the chemical activity of the fluid produced at

the vicinity of the crack tip such that the energy requirements for crack propagation are reduced (*Kerrich et al.*, 1981). However, while it may reduce the size of blocks, it cannot alone accommodate large deformations (*Gratier et al.*, 2013). Stress corrosion is thermally activated but can occur in a broad range of conditions depending of the rock fluid content.

B.4 Dislocation creep

Intracrystalline plasticity is another fundamental deformation mechanism in which grains become internally distorted (*Rutter*, 1986) at high strain rates and over a large temperature range. Dislocation creep, which involves the motion of dislocation through a crystal lattice, is probably the most important mechanism for producing ductile deformation in crystalline materials (*Twiss and Moores*, 1992; *Snoke et al.*, 1998). However, steady-state deformation (creep) involves both a strain-producing process and a recovery process (*Snoke et al.*, 1998). Strain is produced by the glide of line defects (dislocations) through the lattice (unit cell of a grain). The process, called dislocation glide, tends to be brought to a halt by an obstacle (point defect), and this produces strain hardening (*Nicolas and Poirier*, 1976; *Twiss and Moores*, 1992; *Snoke et al.*, 1998). Recovery processes act to offset strain-hardening by allowing the material to restore a state of lower internal energy. Both dislocation glide and recovery processes are thermally activated and depend little on pressure (*Snoke et al.*, 1998). Recovery processes are dislocation climb and dynamic recrystallization processes (subgrain rotation or grain boundary migration) by which new crystals grains form from old grains during deformation processes. Dislocation climb causes the dislocation to climb out of the glide plane (to overcome the point defect) through vacancy diffusion; therefore it is more efficient at high temperatures *Twiss and Moores* (1992). Ductile deformation by dislocation creep produces characteristic microfabrics, including: preferred orientations of mineral crystallographic axes, dislocations microstructures (linear features, undulatory extinction) and grain textures (deformation lamellae, ribbon-shaped grains, subgrains, higly serrated grains boundaries) which varies depending on the strain rate, the temperature and the differential stress undergone by the rock (*Twiss and Moores*, 1992; *Snoke et al.*, 1998). Dislocation creep involves thermal activation, and therefore the process is unlikely to develop before 400°C at the low natural deviatoric stresses (*Rutter*, 1976).

B.5 Twin gliding or mechanical twinning

Twin gliding is another process that involves intracrystalline plasticity, whereby twins are produced from an original structure by simple shearing parallel to the twin plane (*Twiss and Moores*, 1992; *Snoke et al.*, 1998). However, it requires minerals capable of forming twins across its crystallographic planes, and total strains associated with this mechanism are typically not large and depend on the

crystal structure. Great strains must be sustained by other mechanisms (*Twiss and Moores*, 1992; *Burkhard*, 1993; *Snoke et al.*, 1998; *Gratier et al.*, 2013).

B.6 Diffusion creep

The third mechanism that can accommodate creep includes flow by diffusive mass transfer, in which changes of shape of the deforming grains involve the transfer of material from areas of high compressive stress to areas of low compressive stress (*Rutter*, 1986; *Twiss and Moores*, 1992). In the particular case of diffusion creep, the deformation of a crystalline solid takes place by the diffusion of point defects through their crystal lattice (Nabarro-Herring creep) or the the diffusion of atoms or ions along grain boundaries (Coble creep) (*Twiss and Moores*, 1992). Point defects in crystal lattices include both interstitials (extra atoms) and vacancies. The lattice is deformed around interstitials (expand) and vacancies (collapse), creating high-energy defects to be overcomed. With Nabarro-Herring creep, vacancies are created at the surface of the crystal, where the compressive stress is minimum and moves towards the surface of high compressive stress. The flux of atoms is opposite to that of the vacancies, and the shape change of the grain occurs by accumulation of atoms on the low-stressed face (*Twiss and Moores*, 1992). Nabarro-Herring creep is an effective deformation mechanism only at high temperatures and low stress with the strain-rate inversely proportional to the square of the grain size (*Twiss and Moores*, 1992). Coble creep occurs when diffusion (dry) of atoms takes places along the grain boundaries rather than through the volume. Atoms diffuse away from high stressed surfaces to accumulate on a surface of low compressive stress. Coble creep is effective at high temperatures, but lower than for Nabarro-Herring creep, since the diffusion is more rapid because of smaller activation energy (*Twiss and Moores*, 1992). In natural deformation, the minimum temperature, even for very fine grain aggregates, is 500°C for Coble creep and 600°C for Nabarro-Herring (*Rutter*, 1976). Flow law for Coble creep is strongly grain-size dependent, with the strain-rate inversely proportional to the cube of the grain size. Therefore, in both cases (Nabarro-Herring and Coble creep), diffusion creep is suppressed for large grains (*Twiss and Moores*, 1992).

B.7 Pressure-solution creep

Pressure solution is an important deformation mechanism at shallow to intermediate depth in the crust that also involves mass transfer. Deformation of the aggregrate is accomplished by (1) stress-induced dissolution in the presence of fluid at relatively high-stress sites, (2) diffusion through interconnected grain-boundary fluid phase and (3) precipitation at potentially dilatant, low-stress sites (pores, veins) (*Rutter*, 1976; *Robin*, 1978; *Rutter*, 1983; *Gratier et al.*, 2013). Diffusion transfer

may occur at the grain scale or over considerable distances (*Snoke et al.*, 1998). Pressure solution creep is very similar to Coble creep, only the activation energy of fluid phase diffusion is much lower than along dry grain boundaries (*Fischer and Elliott*, 1974; *Twiss and Moores*, 1992; *Gratier et al.*, 2013). Therefore, pressure-solution is the dominant mechanism at temperatures ranging from 20 to $350° - 400°$C, at tectonic strain rate 10^{-10} to 10^{-15} s^{-1} (*Twiss and Moores*, 1992). (*Rutter*, 1976) have inferred that where diffusion is the rate-limiting step, the rate of pressure solution creep should be inversely proportional to the cube of the grain size. There are abundant mircostructral evidences of pressure solution in rocks, found ubiquitously from near the surface down to 10-15 km depth (*Gratier et al.*, 2013). It includes dissolution features (dissolutions seams, stylolites, impressed grains, fossils and pebbles) as well as evidences of precipitations (solution cleavage associated with veins, fibers precipitated in pressure shadows) (*Snoke et al.*, 1998; *Gratier et al.*, 2013).

B.8 Grain-boundary sliding or superplastic creep

Sliding on the grain boundaries can accommodate large strain values; however, it cannot operate alone (*Poirier*, 1985; *Twiss and Moores*, 1992; *Snoke et al.*, 1998; *Gratier et al.*, 2013): there must be an accommodation mechanism to prevent gaps and overlaps at grain boundaries. Therefore, the shape of the grain must change slightly as they pass one another, and this deformation can be accommodated by diffusion or local dislocation motion (*Twiss and Moores*, 1992; *Snoke et al.*, 1998). This mechanism, which has been linked with the development of superplasticity (*Ashby and Verrall*, 1973; *Boullier and Guguen*, 1975; *Konstantinidis and Herrmann*, 1998) is characterized by very rapid strain rates at low stresses compared to other mechanisms of ductile deformation, and a power-law rheology with a stress exponent varying from 1 to 2 (*Twiss and Moores*, 1992). It is traditionally considered as a high-temperature mechanism when sliding is accommodated at dry conditions (*Boullier and Guguen*, 1975; *Gratier et al.*, 2013), so it is not expected to be commonly found in the upper crust. However, *Gratier et al.* (2013) have demonstrated that pressure-solution creep may accommodate grain boundary sliding when a trapped fluid phase activates diffusion along the grain boundary through the entire upper crust.

Appendix C

Nature and origin of the Lichi Mélange

The Lichi Mélange is a $\sim$ 2 km wide formation, cropping out on the western side of the Coastal Range, mainly south of Yuli (Figure 1.5 and 1.6). It is a characteristic block-in-matrix mélange with preferred foliation in a scaly argillaceous matrix and extensional web and boudinage structures in the sandstone blocks (*Chen*, 1997b; *Chang et al.*, 2000). The exotic blocks inside the formation are various in size (millimeters to kilometers) and lithology (arc products, ophiolites, sedimentary rocks). The Lichi Mélange has been intensely studied, and several origins have been proposed. It was first interpreted to be a subduction mélange, developed in the former Manilla Trench during the subduction of the South China Sea oceanic crust (Biq, 1971). But this model is in contradiction with the position of the Lichi Mélange, east of the accretionary wedge (*Huang and Yin*, 1990; *Huang et al.*, 1992; *Reed et al.*, 1992; *Malavieille et al.*, 2002; *Huang et al.*, 2008). Afterwards, it was suggested that the Lichi Mélange was a former olistostrome (*Wang*, 1976; *Ernst*, 1977; *Page and Suppe*, 1981; *Lin and Chen*, 1986) where the sedimentary slumping deposits in the western part of forearc basin were coming from the exposed accretionary prism (proto Central Range). However, marine seismic investigations in the early 1990s combined with previous biostratrigraphic studies, clay composition and lithology of the exotic blocks inside the mélange questioned this model and led instead to the proposal of a tectonic collision origin (*Chang et al.*, 2000, 2001, 2009; *Huang et al.*, 2006a, 2008).

C.1 Marine seismic investigations

Southeastern Taiwan marine seismic investigations in the forearc basin, which lies between the backstop of the accretionary prism and the Luzon arc, have shown key features that help us to understand the origin of the Lichi Mélange. GMGS976 profile at 21N (*Huang et al.*, 2008) (Figure 1.1 and 1.3) shows synchronous deformation and sedimentation in the western part of the forearc basin:

once the sediments are deposited in the Luzon trough, the sequence is deformed and then covered unconformably by the overlying sequence. Consequently, folding and thrusting seem to have occurred since the early history of the forearc sedimentation. On the other hand, in the eastern part of the forearc basin, sedimentation is continuous regardless of active deformation in the west. Further to the north, seismic profiles reveal the progressive closure of the forearc basin by arcward thrusting of the forearc basin strata (*Huang et al.*, 2008; *Malavieille et al.*, 2002; *Reed et al.*, 1992). The accumulation of deformation and shortening of the forearc basin leads to the development of the Huatung Ridge which connects northward with the Lichi Mélange in the southern Coastal Range (Figure 1.1). Those observations support the tectonic collision model where the protolith of the mélange is the forearc basin deposits, and the exotic blocks were incorporated during the early stage of the collision.

C.2 Field observations

Field observations show that the Lichi Mélange lies on the western side of the Coastal Range, mostly in faulting contact with the coherent forearc basin strata and the Tuluanshan (arc) (*Hsu*, 1956; *Teng and Lo*, 1985). Nevertheless, depositional contact between the Lichi and Fanshuliao were reported (*Page and Suppe*, 1981; *Barrier and Muller*, 1984; *Huang et al.*, 2008). Different sheared facies are observed in the Lichi Mélange: from weakly sheared/broken to highly sheared mélange facies (*Chang et al.*, 2000, 2001; *Huang et al.*, 2008). The weakly sheared, broken formation facies still preserves a distinct turbidite sedimentary structure with a basal layer primarily composed of quartz, as in the lower forearc sequences. On the other hand, slate chips, which are commonly found in the upper part of the forearc basin turbidite deposits (< 3 Ma) (*Teng*, 1982), are almost absent in the Lichi Mélange (*Huang et al.*, 2008). Moreover, in the weakly sheared broken facies, we can observe sub-angular to sub-rounded metasandstone conglomerates in pebbly mudstone layers, very similar to the Shuilien Conglomerate, a stratigraphic horizon in the remnant forearc basin sequences of the Coastal Range (*Huang et al.*, 2008; *Page and Suppe*, 1981). Those observations are coherent with a tectonic collision model with reworked material from the forearc basin deposits and its underlying bedrock.

C.3 Constraints from biostratigraphic studies

Biostratigraphic studies have placed a lot of constraints on the origin of the Lichi Mélange (*Chang*, 1967; *Chi et al.*, 1981; *Chi*, 1982; *Barrier and Muller*, 1984; *Huang et al.*, 2008). Planktic foraminifers and calcareous nanoplankton found in the Lichi Mélange and its tributaries show a consistent early Pliocene age which restrains the time of deposition of the protolith to a narrow range (5.5 to 3.7

Ma). Therefore, the Lichi Mélange is coeval with the lower forearc basin sequence, but older than the upper deposits. Consequently, the deformation must have occurred as soon the turbidites were deposited and it was then followed by continuous deposition of younger turbidites (3.5-1 Ma) in the upper part of the forearc basin. This scenario is very similar to what has been deduced from seismic profiles, south of the Coastal Range. Moreover, the benthic foraminifers study of (*Huang et al.*, 2008) have proved that, despite the shearing intensity, microfossils within the Lichi Mélange are similar and compatible with the fauna of the remnant forearc basin to the east. Besides, a comparative study between the Lichi Mélange, the remnant forearc basin strata and the present hemipelagic muds of the North Luzon Trough (Huang, 1993) has shown that the indigenous deep-marine benthic foraminifers are similar in the three formations. Consequently, all of these observations based on the biostratigraphic content of the Coastal Range formations favor a forearc basin protholith for the Lichi Mélange.

C.4 Clay composition

Clay mineral composition (< 2 m) of the muddy matrix and the sedimentary blocks is similar in all samples, regardless of shearing intensity (*Huang et al.*, 2008). They are characterized by illite, chlorite, mixed-layer clay minerals (mica/semectite) and kaolinite (*Lin and Chen*, 1986). Smectite is found as trace or is completely absent. Therefore, the Lichi Mélange must have two sources: one continental, with slightly metamorphosed sediments from the exhumed accretionary prism to provide illite and chlorite, and one volcanic, to derive the kaolinite. The clay mineral assemblage in the turbidites of the remnant forearc basin is very similar in composition except for the kaolinite, which is absent in the Fanshuliao formation (*Lin and Chen*, 1986). *Huang et al.* (2008) claimed that the occurrence of kaolinite shows the tectonic involvement of the volcanic basement beneath the forearc basin, during the formation of the Lichi Mélange. Thrusting, fragmentation and mixing of volcanic rocks within the mélange allowed the incorporation of the kaolinite from the arc formation by fluid flow along the sheared plan or fractures. Therefore, kaolinite is absent in the forearc basin strata because it did not undergo intense deformation.

C.5 Origin of exotic blocks

To understand how the Lichi Mélange was formed, another important matter is the origin of exotic blocks. As mentioned earlier in the text, different lithologies can be observed: arc products, ophiolites and sedimentary deposits. The volcanic products derived from the Luzon volcanic arc include andesite, volcanics breccias, tuffs and volcanoclastic turbidites. Pillow basalts and gabbro, sometimes serpentinized, composed the dismembered ophiolite suite. The larger block (several hundreds of

meters) is known as the East Taiwan Ophiolite (ETO). Ophiolitic blocks appear to be restricted to the intensely sheared facies. They may represent the oceanic crust of either the South China Sea (*Suppe et al.*, 1981; *Jahn*, 1986; *Chung and Sun*, 1992) or the Philippine Sea Plate beneath the Luzon forearc-arc (*Juan et al.*, 1980; *Malavieille et al.*, 2002). The source and emplacing mechanism of these basic products are still highly debated. Microfossil records from intercalated shale within the ophiolites gave an age of 15 Ma (*Huang et al.*, 1979), which is younger than, but close in age, to the youngest South China Sea crust (opening 32-17 Ma) (*Briais et al.*, 1993). However, if the ophiolites came from the South China Sea, it is not clear how they were incorporated within the Lichi Mélange. Indeed, ophiolitic blocks inside the accretionary prism are only observed in the Kenting mélange, *i.e.*, west of the Hengchun Peninsula (southern extension of the Central Range), but not in the Central Range. Moreover, they differ from ETO in composition (*Huang et al.*, 2008). The second potential source of these ophiolites is the basement of either the Luzon arc or the forearc basin. The microfossils are coeval with the age of the Luzon arc formation, which is not older than mid-Miocene (*Huang et al.*, 2008). In that case, ophiolites would have been incorporated within the mélange at the same time as the arc products, during the shortening phase of the forearc basin (Huatung ridge equivalent).

Finally, the sedimentary blocks show two different facies. We can observe weakly lithified Pliocene turbidite units (tens of meters to a kilometer size blocks) with lithology, age and sedimentary turbidite structures simlar to those of the coherent remnants of forearc basin strata of the Coastal Range. The Lichi Mélange also includes metric to kilometric size angular blocks of well-lithified, whitish quartz-rich, feldspathic sandstones. They are late Miocene in age. Zircon fission track studies have shown that they are similar to the non-metamorphosed deep-sea fan sandstones of the upper accretionary prism in the Hengchun Peninsula, but they display a very different age record from the Bouma TA part of the Taiyuan remnant forearc-basin turbidites (*Huang et al.*, 1997, 2008). The whitish sandstone blocks in the Lichi Mélange show a partial annealing feature with two age peaks concentrated at the early-middle Miocene (9-18 Ma) and late Mesozoic (66-130 Ma), whereas the zircon grains in the Fanshuliao formation show either a complete reset (2.08 Ma) or partial reset with a young peak of Pliocene age (2.5 Ma) and an old tail of Mesozoic age (64-100 Ma) (*Huang et al.*, 2008). Those whitish blocks have only been observed in the intensely sheared facies of the Lichi Mélange, not in the weakly sheared, broken facies nor in the remnant forearc basin formation. Consequently, to get a different zircon fission track record and a classification based on shearing intensity, it is hard to imagine that they were delivered to the Lichi Mélange by turbiditic current. They were more probably incorporated by eastward thrusting into the deformed forearc strata (*Huang et al.*, 2008).